

The Effects of Assimilating Satellite Brightness Temperature and Bogus Data on the Simulation of Typhoon Kalmaegi (2008)

WANG Yunfeng^{1,2*} (王云峰), WANG Bin² (王斌), FEI Jianfang¹ (费建芳), HAN Yueqi¹ (韩月琪),
and MA Gang³ (马刚)

¹ Institute of Meteorology and Oceanography, PLA University of Science and Technology, Nanjing 211101

² LASG, Institute of Atmospheric Physics, Chinese Academy of Sciences, Beijing 100029

³ Satellite Meteorological Center, China Meteorological Administration, Beijing 100081

(Received November 26, 2012; in final form March 12, 2013)

ABSTRACT

Observational and bogus satellite data are directly assimilated into the Weather Research and Forecasting (WRF) model in simulations of Typhoon Kalmaegi (2008). The data assimilation is performed using the Radiative Transfer for TIROS-N Operational Vertical Sounder (RTTOV) model and the three-dimensional variational data assimilation (3DVAR) technique, with satellite observations taken from the National Oceanic and Atmospheric Administration-16 (NOAA-16) Advanced TIROS Vertical Sounder (ATOVS) system composed of the High-resolution Infrared Radiation Sounder (HIRS), the Advanced Microwave Sounding Unit-A (AMSU-A), and the Advanced Microwave Sounding Unit-B (AMSU-B). Data assimilation experiments are initialized at three different times. Improvements in the numerical simulation of the typhoon are discussed in the context of wind, temperature, pressure, and geopotential fields.

The results indicate that assimilation of satellite data can improve both the representation of the initial conditions and the subsequent simulation of the typhoon. Different satellite data have different impacts on the typhoon track. In these simulations, data from AMSU-A play a greater role in improving the simulation of the typhoon than data from AMSU-B or HIRS. Assimilation of satellite data significantly affects the simulation of the subtropical high and the steering of the typhoon by the environmental flow. The subtropical high is enhanced and extends westward in the data assimilation experiments. The background flow therefore steers the typhoon more westward, improving the simulated typhoon track. Although direct assimilation of satellite brightness temperature improves the simulated environmental conditions, it does not significantly improve the simulated intensity of the typhoon. By contrast, initializing the typhoon simulation using bogus data in tandem with satellite data improves not only the environmental conditions but also the simulated inner-core structure of the typhoon. Assimilation of both types of data therefore improves the simulation of both the typhoon track and the typhoon intensity. The results of these experiments offer new insight into improving numerical simulations of typhoons.

Key words: WRF model, bogus data, satellite data, 3DVAR

Citation: Wang Yunfeng, Wang Bin, Fei Jianfang, et al., 2013: The effects of assimilating satellite brightness temperature and bogus data on the simulation of Typhoon Kalmaegi (2008). *Acta Meteor. Sinica*, **27**(3), 415–434, doi: 10.1007/s13351-013-0309-2.

1. Introduction

Typhoons are among the most frequent natural disasters that affect human beings. A number of recent studies have focused on the simulation and predictability of typhoons using numerical models (e.g., Chen and Pan, 2010; Cheng et al., 2011; Zhang et

al., 2011; Zhang and Tao, 2013). Accurate predictions of the track and intensity of a typhoon enable effective preventative measures to be enacted in advance, reducing economic losses. Conventional observation data are sparse over the oceans. Objective analyses are therefore typically unable to describe the thermal structure and circulation characteristics of a develop-

Supported by the International Scientific and Technological Cooperation Projects (2010DFA24650), National High-Tech Research and Development (863) Program of China (2010AA012304), China Meteorological Administration Special Public Welfare Research Fund (GYHY201106004), and National Natural Science Foundation of China (41230421, 41105065, and 11271195).

*Corresponding author: wangyf@mail.iap.ac.cn.

ing typhoon precisely. This deficiency is particularly pronounced with respect to the mesoscale structures of typhoons, and results in serious errors in numerical forecasts. The provision of more accurate initial conditions would greatly improve numerical simulations of typhoons, and is therefore an urgent task.

Typhoon forecasts are often initialized using an artificial tropical cyclone (Iwasaki et al., 1987; Mathur, 1991; Kurihara et al., 1993). An ideal bogus typhoon model with elaborate circulation and thermal structures is constructed according to the observational data and then implanted into the environmental fields. This method has been shown to greatly improve the skill of tropical cyclone numerical forecasts, and is widely applied in operational prediction systems in many countries. For example, the well-known Geophysical Fluid Dynamics Laboratory (GFDL) hurricane model is run operationally with a multiply-nested movable mesh (grid resolution as high as 6 km) and a very sophisticated model initialization (Kurihara et al., 1995).

The development and application of the Bogus Data Assimilation (BDA) scheme has expanded the role of idealized bogus data in numerical simulations of typhoons (Zou and Xiao, 2000). Xiao et al. (2000, 2009) showed that the BDA scheme could reduce errors in simulations of both typhoon track and intensity, and Pu and Braun (2001) reported that the assimilation of a bogus vortex played an important role in the adjustment of the initial fields in simulations of hurricanes Georges and Bonnie.

The rapid development of satellite observation systems has enhanced the role of remote sensing data in numerical weather prediction. For example, assimilation of satellite data can greatly improve typhoon initialization schemes. Zou et al. (2001) successfully initialized a typhoon simulation by assimilating Geometry Engine-Open Source (GEOS) observed brightness temperature using the four-dimensional variational assimilation (4DVAR) technique. Their results showed that satellite data assimilation substantially improved simulations of typhoon track, intensity, and precipitation. Le Marshall et al. (2002) reduced the errors in a typhoon track forecast from 400 to 150 km by assimilating high-resolution observations (including satellite

data) into the interior structure of the initial typhoon. Wang et al. (2003) also obtained improved simulations of tropical cyclones by assimilating bogus data, cloud motion winds, and satellite observations into a numerical model using 4DVAR. Zhang et al. (2004) concluded that direct assimilation of AMSU brightness temperature described the three-dimensional structure and evolution of a typhoon better than routine observational data. Zapotocny et al. (2008) also indicated that assimilation of AMSU-A data improved the forecast of a typhoon track, while Wang et al. (2010) showed that the mesoscale structure of a typhoon could be reconstructed in the Mesoscale Model 5 (MM5) using the BDA in tandem with assimilation of AMSU-A brightness temperature data.

In this paper, the BDA and satellite data assimilation techniques are combined to study Typhoon Kalmaegi (2008). The BDA technique used here is comprehensively derived from the work of Mathur (1991), Kurihara et al. (1993, 1995), Wang et al. (1996), and Wang et al. (2009). The assimilated satellite data include observations from the Advanced Microwave Sounding Unit-A (AMSU-A), the Advanced Microwave Sounding Unit-B (AMSU-B), and the High-resolution Infrared Sounder (HIRS) from the National Oceanic and Atmospheric Administration-16 (NOAA-16) Advanced TIROS Vertical Sounder (ATOVS) satellite instrument package. The data assimilation affects both the structure of the environmental fields and the interior structure of the typhoon. Analysis of the optimal initial fields reveals the physical factors that most effectively improve the numerical forecast of the typhoon.

This paper is organized as follows. The numerical model, observational data, and cost function are introduced briefly in Section 2. The experimental design and numerical results are described in Section 3. Section 4 provides a summary of the results and conclusions.

2. Numerical model, observational data, and cost function

2.1 Numerical model

The Weather Research and Forecasting (WRF)

model (version 3.2) and the WRF data assimilation system (WRFDA) are used for the numerical simulations. The Radiative Transfer for TIROS-N Operational Vertical Sounder (RTTOV) version 8.7 modeling system is used to incorporate the ATOVS observations. The WRF model is a fully-compressible non-hydrostatic model with a hydrostatic option. The vertical coordinate is a terrain-following hydrostatic pressure coordinate, and the horizontal grid is an Arakawa C-grid.

The model domain used for this study is centered at 30.0°N , 120.0°E . Two nested domains with grid sizes of 45 km (outer domain) and 15 km (inner domain) are designated (Fig. 1). The grid dimensions are 64×68 and 124×163 for outer and inner domains, respectively. The vertical coordinate consists of 35 η layers. The following physical parameterization schemes are selected in both domains: the WRF Single-Moment 3-class (WSM-3) microphysics scheme, the Rapid Radiative Transfer Model (RRTM) long-wave parameterization (Chou and Suarez, 1999), the Dudhia shortwave parameterization, the Yonsei University (YSU) boundary layer parameterization (Hong et al., 2006), and the updated Kain-Fritsch cumulus parameterization (Kain, 2004).

The WRFDA is an advanced data assimilation system that provides a variety of state-of-the-art 3DVAR/4DVAR and hybrid variational/ensemble data assimilation techniques. The assimilation domains and physical parameterizations used in WRFDA are the same as those used in WRF.

The RTTOV model was originally designed by Eyre and Woolf (1988) and developed at the ECMWF in the early 1990s. It allows the forward simulation of radiances from satellite infrared or microwave nadir-scanning radiometers. Version 8.7 of the RTTOV model includes the complicated nonlinear relationships between satellite brightness temperature and model variables. The WRF model provides the necessary physical parameters to RTTOV. The brightness temperature for each channel is simulated by dividing the atmosphere between 0.1 and 1013.3 hPa into 43 levels based on the real vertical structure of the atmosphere. The transmittance is then calculated level by

level.

2.2 Data

The first-guess field is produced using NCEP/GFS (Global Forecast System) analysis data with a spatial resolution of $1^{\circ} \times 1^{\circ}$. Observations of the typhoon used in the bogus technique are obtained from the best track data provided by the China Meteorological Administration. Bogus data are constructed at standard pressure levels, and then implanted into the initial fields. The typhoon initialization scheme used here is derived from Mathur (1991), Kurihara et al. (1993, 1995), Wang et al. (1996), and Wang et al. (2009). A typhoon-like vortex (which will be referred to as the analyzed vortex) is removed from the analysis and replaced with a specified vortex (which is realistic and compatible with the model). In other words, the initial field is given by the global analysis minus the analyzed vortex plus the specified vortex. The method for removing the analyzed vortex follows Kurihara et al. (1993, 1995), and the method for determining and adding the specified vortex follows Mathur (1991), Wang et al. (1996), and Wang et al. (2009).

The sea level pressure (SLP) and wind fields are

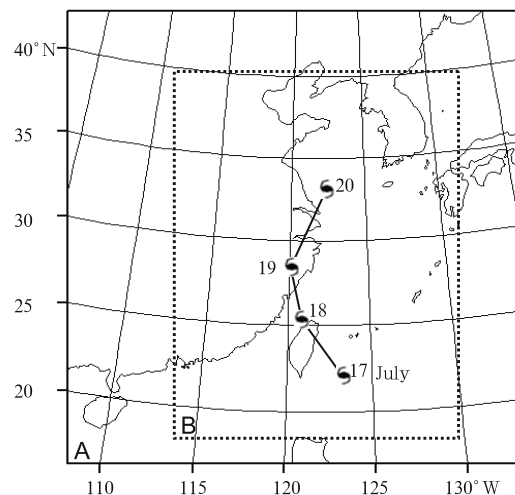


Fig. 1. The observed best track of Typhoon Kalmaegi between 0000 UTC 17 and 0000 UTC 20 July 2010. Domains A and B indicate the outer and inner domains used in this study.

constructed using the following equations:

$$P_0(r) = P_c + \Delta P \left\{ 1 - \left[1 + \frac{1}{2} \left(\frac{r}{R} \right)^2 \right]^{-\frac{1}{2}} \right\}, \quad (1)$$

$$V_0(r) = \left(\frac{r}{\rho} \frac{\partial P_0}{\partial r} + \frac{f^2 r^2}{4} \right)^{\frac{1}{2}} - \frac{r|f|}{2}, \quad (2)$$

where P_c is the central SLP of the observed typhoon, ΔP is a parameter related to the typhoon SLP gradient (as determined by the maximum wind), R is the radius of the maximum SLP gradient (which usually corresponds to the maximum wind), r is the radius of the vortex, and ρ is air density. The SLP and wind fields are then assimilated into the numerical model

using the 3DVAR technique. For Typhoon Kalmaegi at 0000 UTC 17 July 2008, $P_c = 975$ hPa, $V_{\max} = 33$ m s⁻¹, and $R = 80$ km.

The satellite data are taken from NOAA-16 ATOVS (HIRS, AMSU-A, and AMSU-B), as provided by the National Aeronautics and Space Administration (NASA). HIRS has a total of 20 channels, AMSU-A has a total of 15 channels, and AMSU-B has a total of 5 channels. Quality control, channel selection, and cloud identification are performed according to the default settings in the WRFDA model. Bias correction and data thinning are not applied. Figure 2 shows the distributions of AMSU-A channel 5 brightness temperatures at 2016 UTC 16, 2152 UTC 16, and

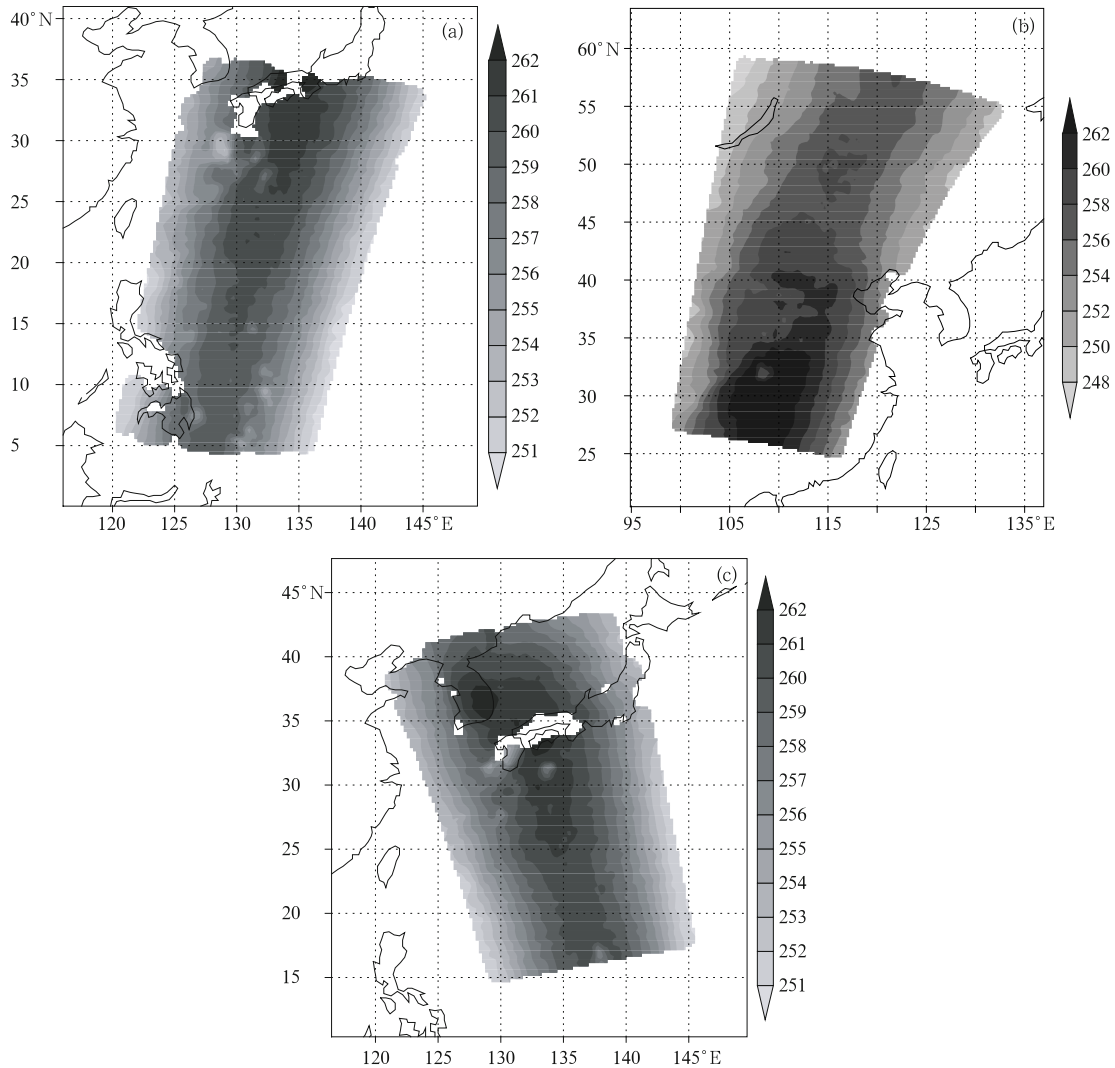


Fig. 2. Distributions of AMSU-A channel 5 brightness temperatures (K) at (a) 2016 UTC 16, (b) 2152 UTC 16, and (c) 0734 UTC 17 July 2008.

0734 UTC 17 July 2008. The distributions of brightness temperatures observed by HIRS and AMSU-B are similar to those observed by AMSU-A (figure omitted).

2.3 Cost function

The cost function for the 3DVAR multifold (bogus, HIRS, AMSU-A, and AMSU-B) data assimilation experiments is defined as

$$J = J_B + J_{\text{Bogus}} + J_{\text{HIRS}} + J_{\text{AMSUA}} + J_{\text{AMSUB}}, \quad (3)$$

where J_B is the difference between the model control variable X and the background variable X_B , J_{Bogus} is the difference between the simulated and observed bogus data, J_{HIRS} is the difference between the simulated and observed HIRS data, and so on. These variables are defined as follows.

$$J_B = \frac{1}{2} \sum_i (X - X_B)^T \mathbf{B}^{-1} (X - X_B), \quad (4)$$

$$J_{\text{Bogus}} = \frac{1}{2} \sum_i \{ [P(r) - P_0(r)]^T \mathbf{O}_P^{-1} [P(r) - P_0(r)] + [V(r) - V_0(r)]^T \mathbf{O}_V^{-1} [V(r) - V_0(r)] \}, \quad (5)$$

$$J_{\text{HIRS}} = \frac{1}{2} \sum_i [H_{\text{HIRS}}(X) - \text{BT}_{\text{HIRS}}]^T \mathbf{O}_{\text{HIRS}}^{-1} \cdot [H_{\text{HIRS}}(X) - \text{BT}_{\text{HIRS}}], \quad (6)$$

$$J_{\text{AMSUA}} = \frac{1}{2} \sum_i [H_{\text{AMSUA}}(X) - \text{BT}_{\text{AMSUA}}]^T \cdot \mathbf{O}_{\text{AMSUA}}^{-1} [H_{\text{AMSUA}}(X) - \text{BT}_{\text{AMSUA}}], \quad (7)$$

$$J_{\text{AMSUB}} = \frac{1}{2} \sum_i [H_{\text{AMSUB}}(X) - \text{BT}_{\text{AMSUB}}]^T \cdot \mathbf{O}_{\text{AMSUB}}^{-1} [H_{\text{AMSUB}}(X) - \text{BT}_{\text{AMSUB}}], \quad (8)$$

where the superscript T represents matrix transpose, \mathbf{B} is the background error covariance matrix, $P(r)$ and $V(r)$ represent the simulated SLP and wind fields, respectively, \mathbf{O}_P and \mathbf{O}_V are the error covariance matrices for the SLP and wind fields, respectively, symbol \sum represents summation, and subscript i represents different observation points at the same time. H_{HIRS} , H_{AMSUA} , and H_{AMSUB} are forward radiative transfer

operators for HIRS, AMSU-A, and AMSU-B, respectively. BT represents the brightness temperature and \mathbf{O} the error covariance matrix of the observed satellite data, with the satellite instrument indicated by the subscript.

3. Numerical experiments

3.1 Typhoon Kalmaegi (2008)

Typhoon Kalmaegi (2008) formed over the ocean northeast of the Philippines on 15 July 2008. It then moved toward the Taiwan Island, making a direct landfall in northern Taiwan Region at 1500 UTC 17 July 2008 before emerging into the Taiwan Strait. The typhoon made a second landfall in Fujian Province at 1200 UTC 18 July 2008, with wind speed of approximately 23 m s^{-1} . It moved into the Yellow Sea and raced toward the Korean Peninsula shortly afterwards, eventually moving inland over North Korea.

This study emphasizes the evolution of the typhoon, its track, and its landing position. The data assimilation experiments are initialized at three times: 1800 UTC 16, 0000 UTC 17, and 0600 UTC 17 July. Each forecast is integrated for 72 h.

3.2 Satellite data assimilation

3.2.1 Experimental design

The effect of satellite data assimilation is studied through three control experiments (Ctrl_00, Ctrl_06, and Ctrl_12) and 21 assimilation experiments (7 at each of the 3 initialization times), as described in Table 1. The initial fields for the control runs are from the NCEP data, with no assimilation of satellite brightness temperature. Different sets of satellite brightness temperature data are assimilated in each of the assimilation experiments. The assimilation time windows are set as $[-4 \text{ h}, +4 \text{ h}]$ to enable the assimilation of more satellite observations.

3.2.2 Typhoon track simulation

Figure 3 shows the typhoon tracks simulated by the different experiments with initialization times at 1800 UTC 16, 0000 UTC 17, and 0600 UTC 17 July. The observed typhoon track (denoted by the typhoon symbol) has four characteristics: (1) the typhoon mak-

Table 1. Numerical data assimilation experiments

Initialization time	1800 UTC July 16	0000 UTC July 17	0600 UTC July 17	Assimilated data
	Ctrl_00	Ctrl_06	Ctrl_12	None
	AMSUA_00	AMSUA_06	AMSUA_12	AMSU-A
	AMSUB_00	AMSUB_06	AMSUB_12	AMSU-B
	HIRS_00	HIRS_06	HIRS_12	HIRS
	ALLSAT_00	ALLSAT_06	ALLSAT_12	AMSU-A, AMSU-B, HIRS
Experiments	AMSUA/AMSUB_00	AMSUA/AMSUB_06	AMSUA/AMSUB_12	AMSU-A, AMSU-B
	AMSUA/HIRS_00	AMSUA/HIRS_06	AMSUA/HIRS_12	AMSU-A, HIRS
	AMSUB/HIRS_00	AMSUB/HIRS_06	AMSUB/HIRS_12	AMSU-B, HIRS

Note: NCEP/GFS analysis data are used as the initial fields.

es its first landfall in Taiwan, (2) the typhoon lands in Fujian Province after passing through the Taiwan Strait, (3) the typhoon turns northeastward after landing in mainland China, and (4) the typhoon moves out into the sea. The tracks simulated by the control runs (Ctrl_00, Ctrl_06, and Ctrl_12) diverge substantially from the observed track, and the above characteristics of the actual typhoon track are not captured accurately.

Figures 3a and 3b show the results of the experiments initialized at 1800 UTC 16 July. The assimilation of AMSU-A data moves the simulated typhoon track (AMSUA_00) closer to the observed track relative to the control experiment (Ctrl_00); however, the simulated typhoon still does not make landfall in Taiwan. The simulated typhoon does make landfall in mainland China, but the landing position is about 350 km from the best track. The assimilation of AMSU-B data (AMSUB_00) offers no obvious improvement over the control run. In fact, the performance of AMSUB_00 is worse than that of Ctrl_00 at some times. The assimilation of HIRS data (HIRS_00) also offers no obvious improvement, with the simulated typhoon missing both the Taiwan Region and mainland China. Assimilating all the satellite data (ALLSAT_00) improves the simulated track of the typhoon substantially. Although the simulated typhoon still does not land in the Taiwan Region, it does land in mainland China (although this landing misses the actual location by about 250 km). The

tracks from experiments AMSUA/AMSUB_00 and AMSUA/HIRS_00 provide even greater improvement over the control simulation, whereas the track from AMSUB/HIRS_00 offers no obvious improvement.

Figures 3c and 3d show the results of the experiments initialized at 0000 UTC 17 July. Those assimilating only HIRS or AMSU-B data again indicate little or no improvement in the typhoon track relative to the control run. However, assimilation of the AMSU-A data either alone or together with other satellite data improves the simulated typhoon track substantially. The simulated typhoon lands in both the Taiwan Region and mainland China when AMSU-A data are assimilated, with landing positions very close to the observed.

Figures 3e and 3f show the results of the experiments initialized at 0600 UTC 17 July. As above, the tracks of the simulated typhoon are closer to the best track for experiments that assimilate AMSU-A data (AMSUA_12, AMSUA/AMSUB_12, AMSUA/HIRS_12, and ALLSAT_12). The simulated landing positions in AMSUA_12 and AMSUA/AMSUB_12 are approximately 200 km away from the best track, and even closer for ALLSAT_12 and AMSUA/HIRS_12. By contrast, the assimilation of HIRS or AMSU-B data alone offers little improvement in the simulated typhoon track. Assimilation of AMSU-A data improves forecasts of this typhoon more effectively than assimilation of AMSU-B or HIRS data.

Figure 4 shows the errors in the tracks simulated by different experiments. The control experiments

(Ctrl_00, Ctrl_06, and Ctrl_12) all produce substantial errors relative to the best track. These errors

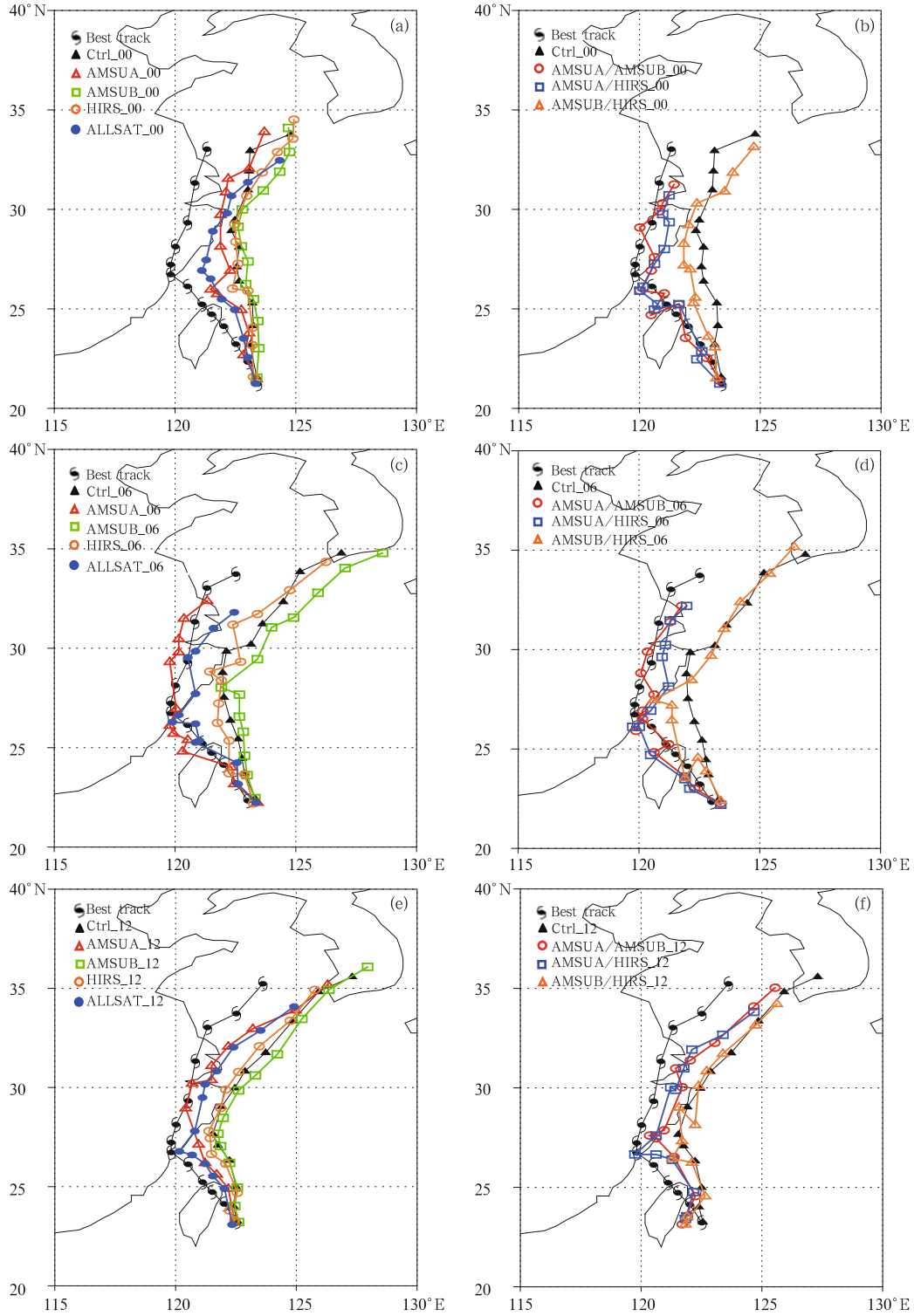


Fig. 3. Typhoon tracks simulated by different data assimilation experiments (shown in Table 1) with initialization times at (a, b) 1800 UTC 16, (c, d) 0000 UTC 17, and (e, f) 0600 UTC 17 July.

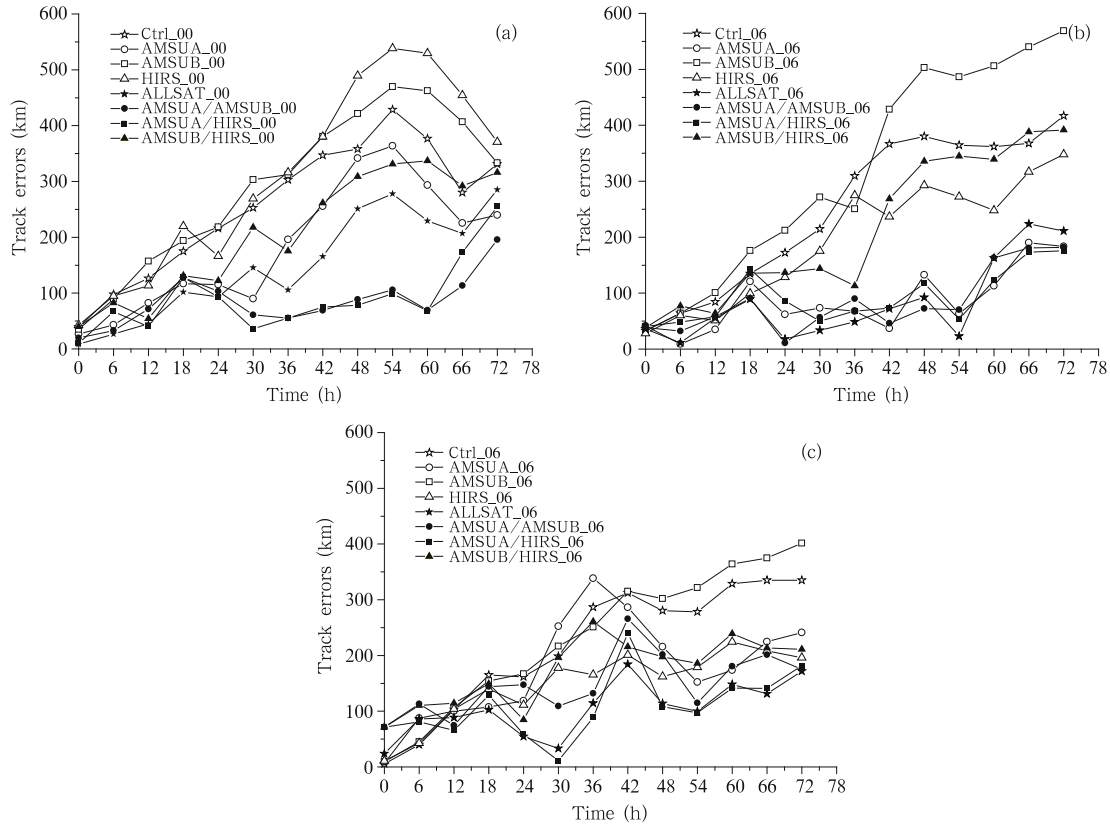


Fig. 4. Errors in simulated typhoon tracks relative to the best track for experiments with initialization times at (a) 1800 UTC 16, (b) 0000 UTC 17, and (c) 0600 UTC 17 July.

tend to increase with time. The largest error for Ctrl_00 is greater than 400 km (at 54 h), the largest error for Ctrl_06 is also greater than 400 km (at 72 h), and the largest error for Ctrl_12 is approximately 350 km (at 72 h).

The errors in the typhoon tracks simulated by different experiments initialized at 1800 UTC 16 July are shown in Fig. 4a. The largest errors in the tracks simulated by experiments HIRS_00 and AMSUB_00 are larger than those simulated by Ctrl_00. The largest error is nearly 550 km when only the HIRS data are assimilated, and 450 km when only the AMSU-B data are used. The largest error is substantially lower (350 km) when AMSU-A data are assimilated alone, and lower still (about 300 km) when all of the satellite data are assimilated (experiment ALLSAT_00). The errors in the typhoon tracks simulated by AMSUA/AMSUB_00 and AMSUA/HIRS_00 are also much smaller than the er-

rors associated with Ctrl_00.

The errors in the typhoon tracks simulated by the experiments initialized at 0000 (0600) UTC 17 July are shown in Fig. 4b (Fig. 4c). The errors in typhoon tracks from the data assimilation experiments are smaller than those from the control runs (Ctrl_06 and Ctrl_12). Experiments that assimilate AMSU-A data generally have smaller track errors.

3.2.3 Typhoon intensity simulation

Figure 5 shows variations in the observed and simulated central SLPs in different assimilation experiments initialized at 0000 UTC 17 July. The observed central SLP is 975 hPa at the initial time, and then gradually increases to 998 hPa at the final time. The central SLP in the control experiment is always relatively weak, with fluctuations around 1000 hPa. The assimilation of ATOVS data offers no obvious improvement in the simulated central SLP. The model only assimilates satellite data under clear-sky conditions,

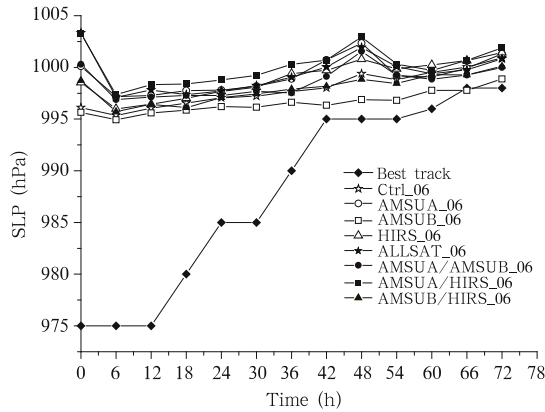


Fig. 5. Variations of the observed and simulated central SLPs in different assimilation experiments initialized at 0000 UTC 17 July.

with satellite brightness temperature data near the typhoon center eliminated during data quality control. It is therefore difficult to improve simulations of typhoon intensity solely by assimilating satellite data.

3.2.4 Typhoon initial fields

The simulated typhoon track is closely related to the initial wind fields. Figure 6 shows differences in the initial wind fields at 500 hPa between the assimilation and the control experiment initialized at 0000 UTC 17 July. The distribution of the initial wind field at 500 hPa in the control experiment (Fig. 6a) shows that Typhoon Kalmaegi is located to the east of the Taiwan Region with a maximum wind speed of 30 m s^{-1} near the typhoon center. For brevity, differences are only shown for the assimilation experiments AMSUA_06, AMSUB_06, HIRS_06, and ALLSAT_06.

Assimilation of AMSU-A data introduces a clockwise anticyclonic anomaly centered at 32°N , 118°E at 500 hPa (Fig. 6b). The difference in the maximum wind speed near the typhoon center is 5 m s^{-1} or so. This anticyclonic anomaly acts to decrease the intensity of the simulated typhoon, but it also embeds the typhoon in a more westward environmental flow. The typhoon simulated in experiment Ctrl_06 is located east of the best track, so this more westward environmental flow pushes the track of the simulated typhoon closer to the best track. This enables AMSUA_06 to more accurately capture the characteristics of the observed typhoon track, i.e., the first landfall in the

Taiwan Region and second over mainland China as well as the subsequent right turn and return to the ocean. Assimilating AMSU-B data introduces a cyclonic anomaly at 500 hPa (Fig. 6c), with a difference of about 3 m s^{-1} in the maximum wind speed near the typhoon center. This cyclonic wind anomaly increases the intensity of the simulated typhoon, but prevents it from moving westward.

Assimilating HIRS data introduces an anticyclonic vortex over the ocean to the east of the Taiwan Region (Fig. 6d). The change in the maximum wind speed near the typhoon center is approximately 2 m s^{-1} . This anticyclonic anomaly decreases the intensity of the simulated typhoon. These differences in the initial wind field will initially push the typhoon westward, but turn the typhoon toward the right earlier than observed, when the typhoon approaches the Taiwan Region. Assimilation of HIRS data therefore makes the simulated typhoon track more accurate at the beginning of the simulation, but offers little improvement during later periods.

The difference in the initial wind field when all satellite data are assimilated (Fig. 6e) is very similar to that when only AMSU-A data are assimilated (Fig. 6b), although the locations of the anticyclonic anomalies are somewhat different between the two cases. This similarity in the changes of the initial wind field between ALLSAT_06 and AMSUA_06 results in similar modifications to the track of the simulated typhoon, again leading to a more accurate characterization of the observed track than in the control case. As in AMSUA_06, the difference in the maximum wind speed near the typhoon center is about 5 m s^{-1} .

Figure 7a shows the initial vertical distribution of geopotential along 22°N in Ctrl_06. The magnitude ranges approximately 10^4 – $10^5 \text{ m}^2 \text{ s}^{-2}$ over the free troposphere. Assimilating AMSU-A data (Fig. 7b) or HIRS data (Fig. 7d) introduces a positive increment in geopotential in the lower and mid troposphere near the typhoon center (22°N , 123°E), which acts to decrease the initial intensity of the typhoon. The effect of assimilating AMSU-B data (Fig. 7c) is the opposite, with negative geopotential increments in the lower and mid troposphere that act to increase the initial inten-

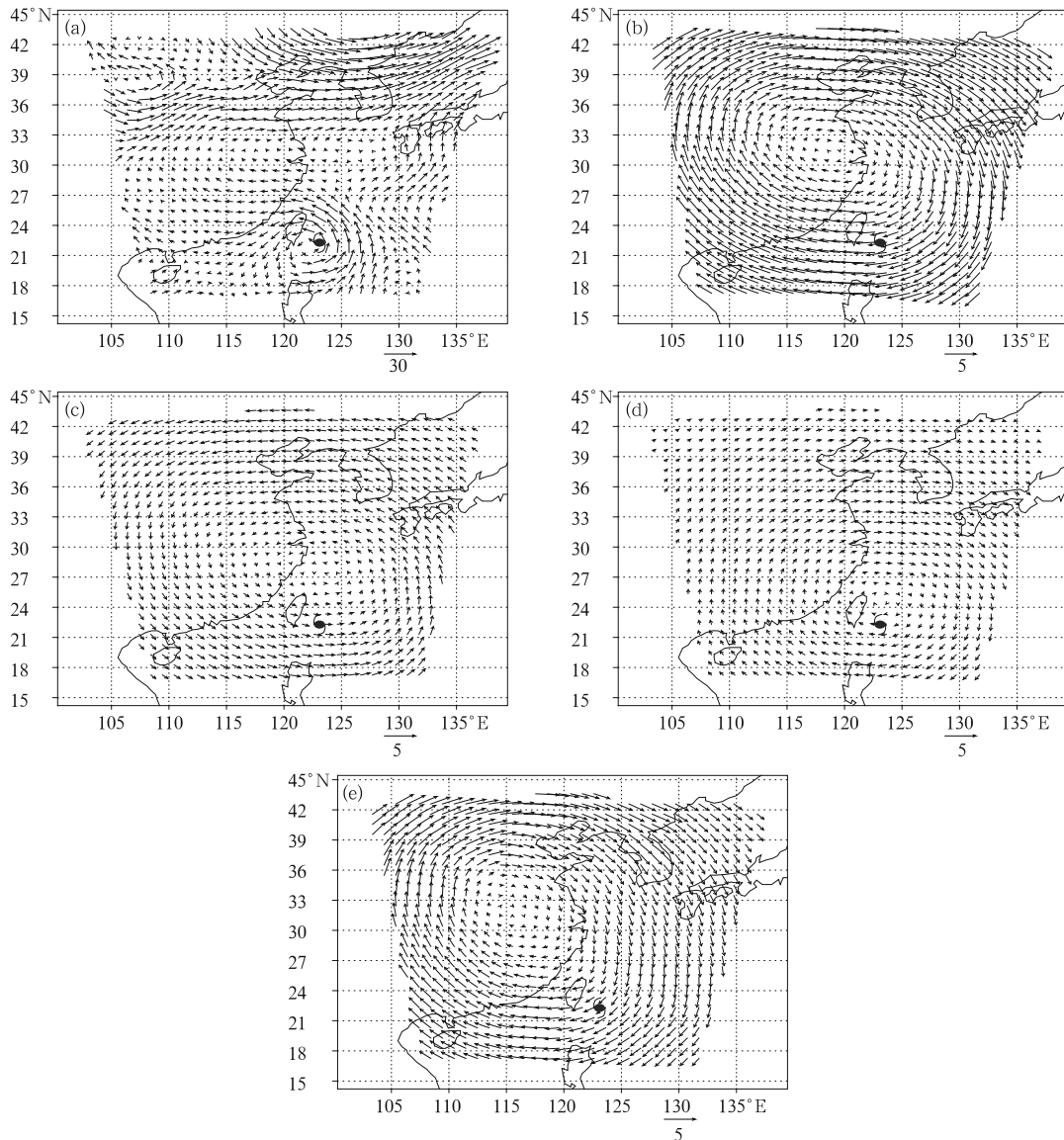


Fig. 6. Distributions of the initial wind field (m s^{-1}) at 500 hPa in experiment Ctrl_06 and differences in that between Ctrl_06 and the various assimilation experiments initialized at 0000 UTC 17 July. (a) Ctrl_06, (b) AMSUA_06 – Ctrl_06, (c) AMSUB_06 – Ctrl_06, (d) HIRS_06 – Ctrl_06, and (e) ALLSAT_06 – Ctrl_06.

sity of the typhoon. The effect of assimilating the multifold satellite data (Fig. 7e) is qualitatively similar to the effect of assimilating only AMSU-A (Fig. 7b), but the amplitude of the changes in geopotential is larger when all three sets of satellite data are assimilated. The subtropical high is located near 26°N . An enhancement of the initial geopotential in the lower and mid troposphere can therefore intensify the subtropical high and cause it to extend westward. The changes in geopotential in Fig. 7 also correspond to

the changes in central SLP in Fig. 5.

Figure 8a shows the initial distributions of geopotential at 500 hPa for Ctrl_06 and ALLSAT_06. Assimilating all satellite data increases the initial geopotential, strengthening the subtropical high, and causing it to extend westward. The intensification of the subtropical high promotes the initial westward movement of the simulated typhoon. The westward extension of the subtropical high contributes to the subsequent right turn and northward movement of the

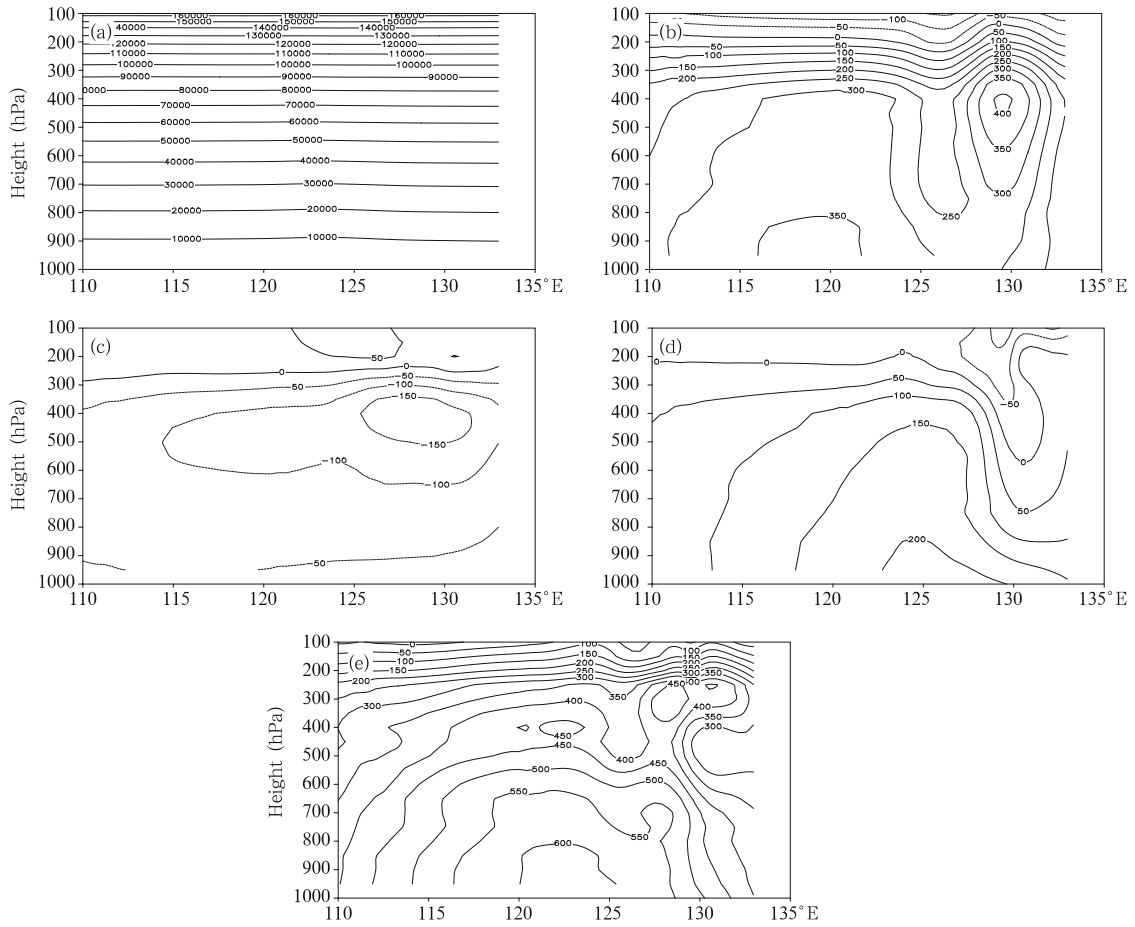


Fig. 7. As in Fig. 6, but for the initial vertical distributions of geopotential ($\text{m}^2 \text{s}^{-2}$) along 22°N .

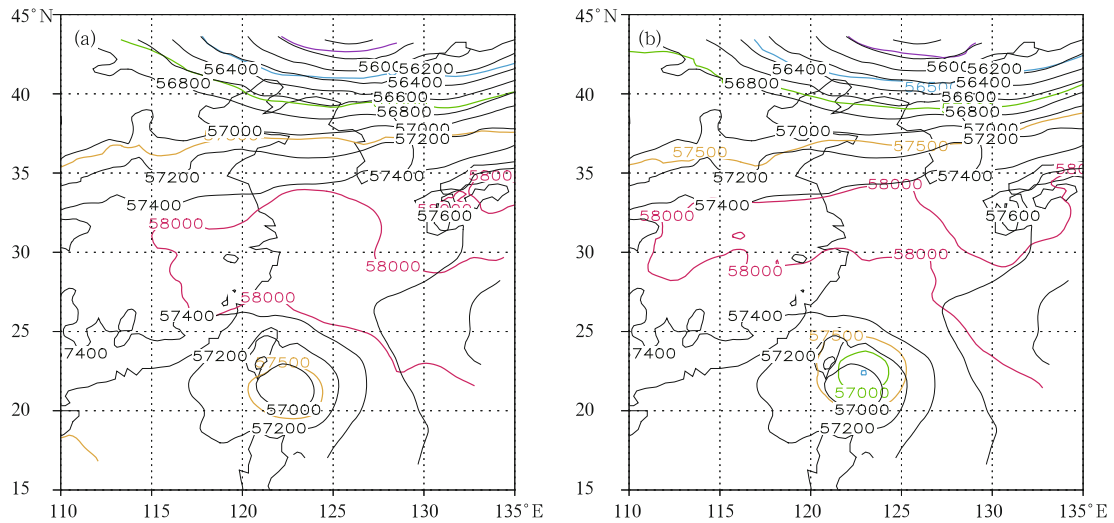


Fig. 8. Distributions of geopotential ($\text{m}^2 \text{s}^{-2}$) at 500 hPa for the control experiment Ctrl-06 (black contours) and for the multifold satellite assimilation experiments (colored contours) initialized at 0000 UTC 17 July (a) without the bogus technique and (b) with the bogus technique.

typhoon.

Figure 9a shows the initial vertical distributions of temperature along 22°N in Ctrl_06. Its magnitude is on the order of 10^2 K. The assimilation of satellite data mainly changes the vertical distribution of temperature between 122° and 134°E (Figs. 9b–9e). This is the area that was covered by the satellite orbit at 2016 UTC 16 July 2008 (Fig. 2a). Assimilating AMSU-A data (Fig. 9b) leads to increases of temperature in the lower and mid troposphere and decreases of temperature in the upper troposphere near 130°E. Wang et al. (2010) also showed a decrease in temperature at upper levels after assimilating AMSU-A data using the 4DVAR technique. The changes in temperature in the lower and mid troposphere can enhance the subtropical high and are therefore helpful in promoting the westward movement of the simulated typhoon. Assimilating AMSU-B data (Fig. 9c) or HIRS data (Fig. 9d) leads to qualitatively opposite changes in the

vertical distribution of temperature: decreases in the lower and mid troposphere near 130°E but increases in the upper troposphere. Assimilation of all satellite data (Fig. 9e) leads to very complicated changes in the vertical distribution of temperature. The final results represent the combined effect of the individual satellite data sets, with alternating increases and decreases in temperature over the area near 130°E. Because of the complexity of the temperature increment, the simulated typhoon track should be considered in the context of other physical fields (Figs. 6–8).

3.3 Satellite data assimilation together with the bogus technique

3.3.1 Experimental design

Three control experiments (Bogus_00, Bogus_06, and Bogus_12) and 21 experiments are designed to study the impact of satellite data assimilation in tandem with the bogus technique (Table 2). As before,

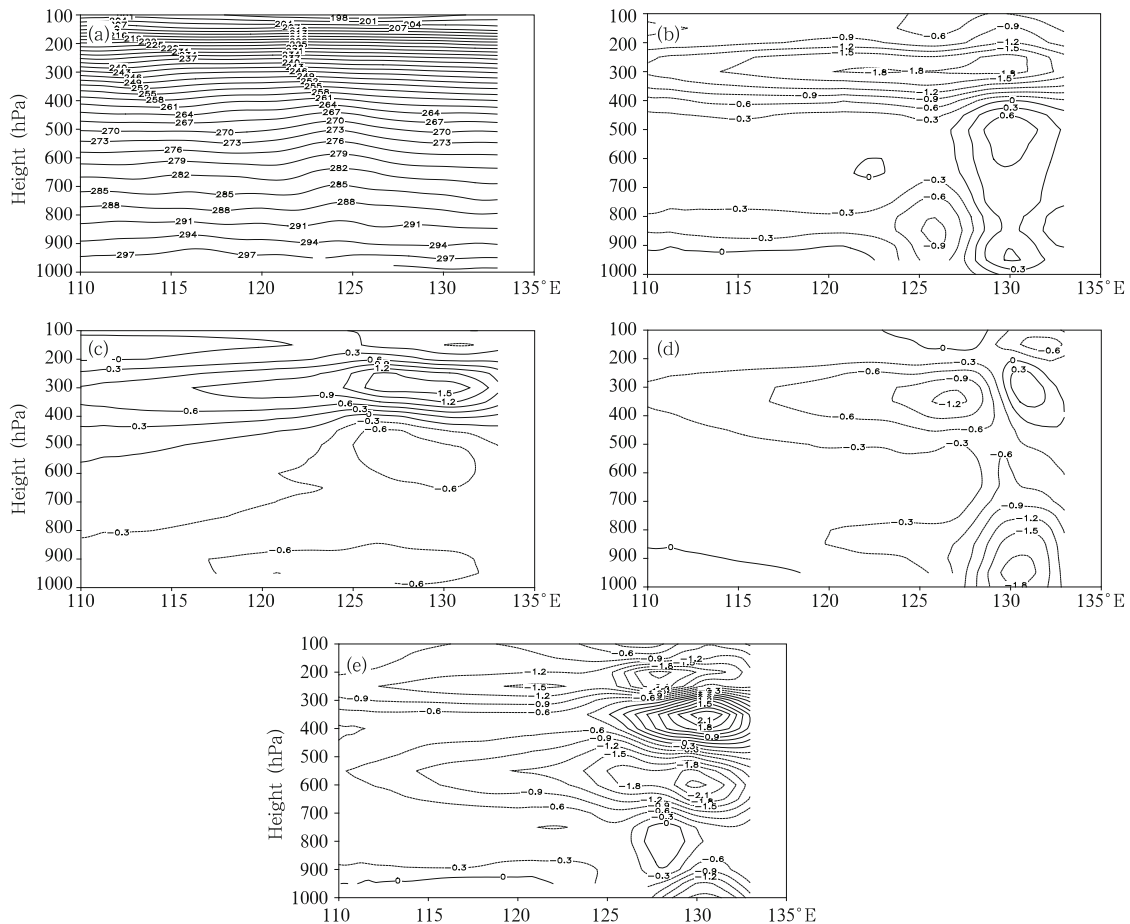


Fig. 9. As in Fig. 7, but for temperature (K).

Table 2. Numerical experiments assimilating the bogus data, SLP data, and sea level wind data

Initialization time	1800 UTC 16 July	0000 UTC 17 July	0600 UTC 17 July	Assimilated data
	Bogus_00	Bogus_06	Bogus_12	None
	B_AMSUA_00	B_AMSUA_06	B_AMSUA_12	AMSU-A
	B_AMSUB_00	B_AMSUB_06	B_AMSUB_12	AMSU-B
	B_HIRS_00	B_HIRS_06	B_HIRS_12	HIRS
	B_ALLSAT_00	B_ALLSAT_06	B_ALLSAT_12	AMSU-A, AMSU-B, HIRS
Experiments	B_AMSUA/AMSUB_00	B_AMSUA/AMSUB_06	B_AMSUA/AMSUB_12	AMSU-A, AMSU-B, HIRS
	B_AMSUA/HIRS_00	B_AMSUA/HIRS_06	B_AMSUA/HIRS_12	AMSU-A, HIRS
	B_AMSUB/HIRS_00	B_AMSUB/HIRS_06	B_AMSUB/HIRS_12	AMSU-B, HIRS

3 sets of 8 experiments are initialized at 1800 UTC 16, 0000 UTC 17, and 0600 UTC 17 July, respectively. The bogus data on standard levels are constructed and implanted into the initial fields, while SLP and sea level wind data are constructed and assimilated into the model by using the 3DVAR technique. Satellite data are also assimilated into the model by using the 3DVAR technique. The physical parameters used in these experiments are identical to those used in the experiments listed in Table 1.

3.3.2 Typhoon track

Figure 10 shows the typhoon tracks simulated by the combined bogus and data assimilation experiments initialized at 1800 UTC 16, 0000 UTC 17, and 0600 UTC 17 July. The typhoon tracks simulated by the control runs with bogus data (Bogus_00, Bogus_06, and Bogus_12) are closer to the best track than those simulated by the control runs without bogus data (Ctrl_00, Ctrl_06, and Ctrl_12). The bogus data and the BDA technique are applied in all the data assimilation runs listed in Table 2. The remainder of this section will focus on the effects of assimilating different combinations of satellite data.

Figures 10a and 10b show the tracks from the experiments initialized at 1800 UTC 16 July. The track from Bogus_00 is better than that from Ctrl_00, with TC landings on both the northern coast of the Taiwan Island and mainland China (although the exact landing locations differ and are incorrect). The track from Bogus_00 is to the east of the best track. Assimilation of AMSU-A data (B_AMSUA_00) shifts the

simulated typhoon track to the west of the best track. The simulated landings are to the south of the observed ones, and the simulated typhoon moves more slowly than the observation. The track simulated by B_AMSUB_00 is largely consistent with the observed track at the beginning of the simulation, and the simulated typhoon lands in the Taiwan Region at nearly the same location as the actual typhoon. The simulated typhoon moves in a wrong direction after its first landing, however; so it lands at a wrong location when it reaches mainland China. Furthermore, the simulated typhoon moves too fast and returns to the ocean earlier than the observation.

Assimilating HIRS data (B_HIRS_00) results in a simulated typhoon firstly landing to the south of the observed location, but largely consistent with the best track for its second landing over mainland China. The position where the simulated typhoon moves back to the ocean again is to the south of the best track. Assimilating all satellite data (B_ALLSAT_00) results in a typhoon track that is between the tracks simulated by B_HIRS_00 and B_AMSUA_00. This indicates that the simulated typhoon track reflects the combined effects of the multifold satellite data. The track simulated when AMSU-B and HIRS data are assimilated in tandem (B_AMSUB/HIRS_00) has substantial errors relative to the best track. By contrast, B_AMSUA/AMSUB_00 and B_AMSUA/HIRS_00 yield more accurate tracks than Bogus_00.

The tracks simulated by the experiments initialized at 0000 UTC 17 July are shown in Figs. 10c and

10d. The track from Bogus_06 is considerably closer to the best track than that from Ctrl_06. The simulated typhoon makes its first landfall at almost the

same location as the observation, but its second landing position in mainland China is incorrect. The tracks from B_AMSUB_06, B_AMSUB/HIRS_06, and

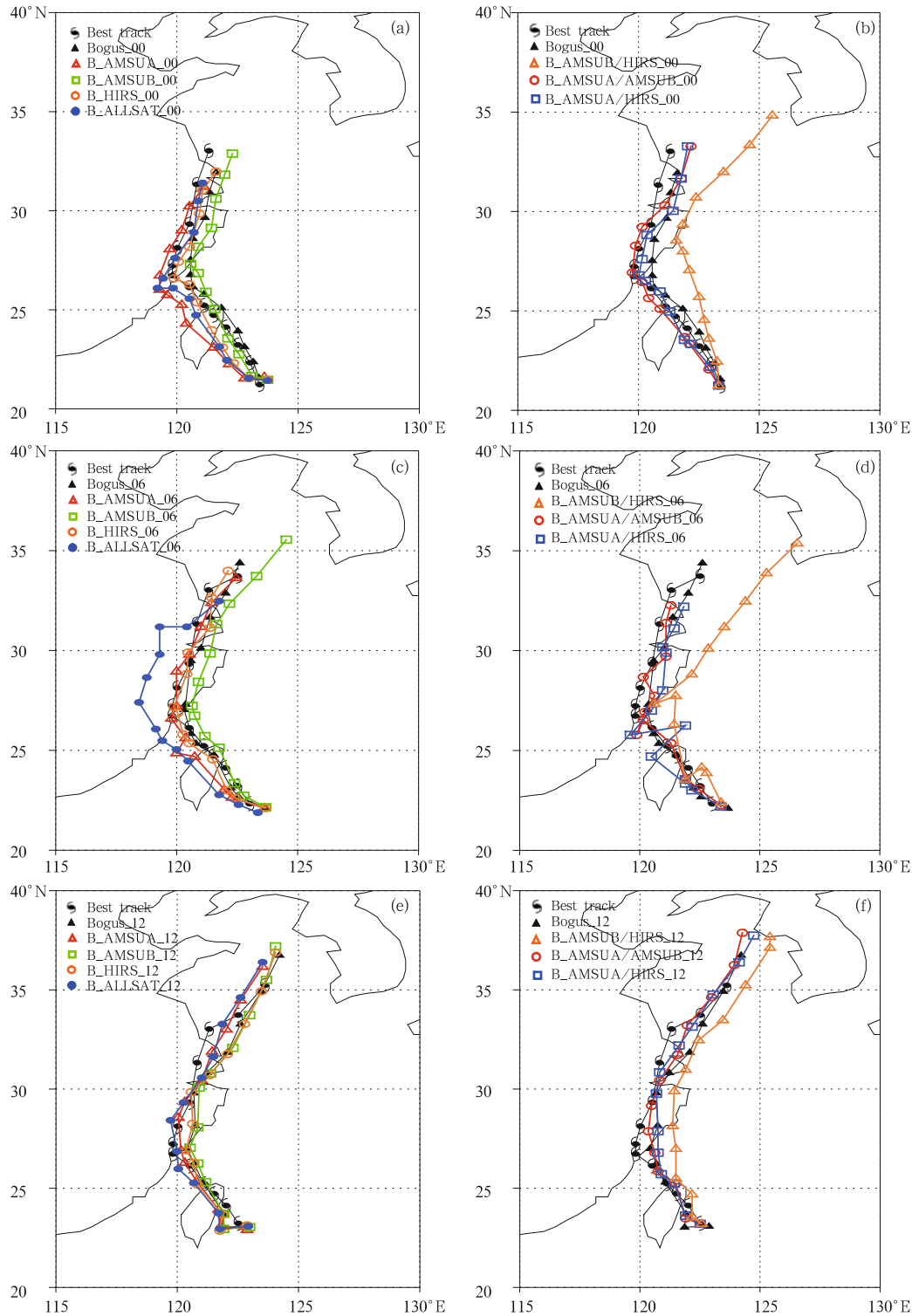


Fig. 10. As in Fig. 3, but for the combined bogus and satellite data assimilation experiments (shown in Table 2).

B_ALLSAT_06 are worse than that from Bogus_06. Satellite data assimilation has a positive effect on the simulations of typhoon track in all other experiments.

The typhoon tracks simulated by the experiments initialized at 0600 UTC 17 July are shown in Figs. 10e and 10f. The track in Bogus_12 is again closer to the best track than that in Ctrl_12. The simulated first landing position is almost the same as the best track, but the second landing location is again incorrect. The simulated typhoon tracks are improved by satellite data assimilation in all experiments except B_AMSUB/HIRS_12. Experiment B_ALLSAT_12 gives the most accurate typhoon track.

Figure 11 shows the track errors associated with the bogus data experiments. The errors in the tracks simulated by the three control runs with bogus data (Bogus_00, Bogus_06, and Bogus_12) are smaller than the three control runs without bogus data (Ctrl_00, Ctrl_06, and Ctrl_12). The largest errors in the control runs with bogus data are approximately 200 km.

The errors in the tracks from the experiments initialized at 1800 UTC 16 July are shown in Fig. 11a. Assimilating HIRS data improves the track simulation significantly. The errors in B_HIRS_00 increase gradually throughout the simulation, but are always less than 130 km. The errors in B_AMSUA_00 are much smaller than those in Ctrl_00 (Fig. 4a), with a maximum error of approximately 200 km. However, these errors are comparable to those in Bogus_00. The errors in B_AMSUB_00 are consistently less than 100 km over the first 54 h, and the errors between 54 and 72 h are still less than 200 km. Assimilating all satellite data (B_ALLSAT_00) yields track errors of less than 120 km over the first 66 h and less than 180 km over the full 72-h period. The errors in B_AMSUA/AMSUB_00 and B_AMSUA/HIRS_00 are sometimes smaller and sometimes larger than those in Bogus_00, with a maximum error of less than 140 km. The errors in B_AMSUB/HIRS_00 are far larger than those in Bogus_00, with a maximum of approximately 420 km.

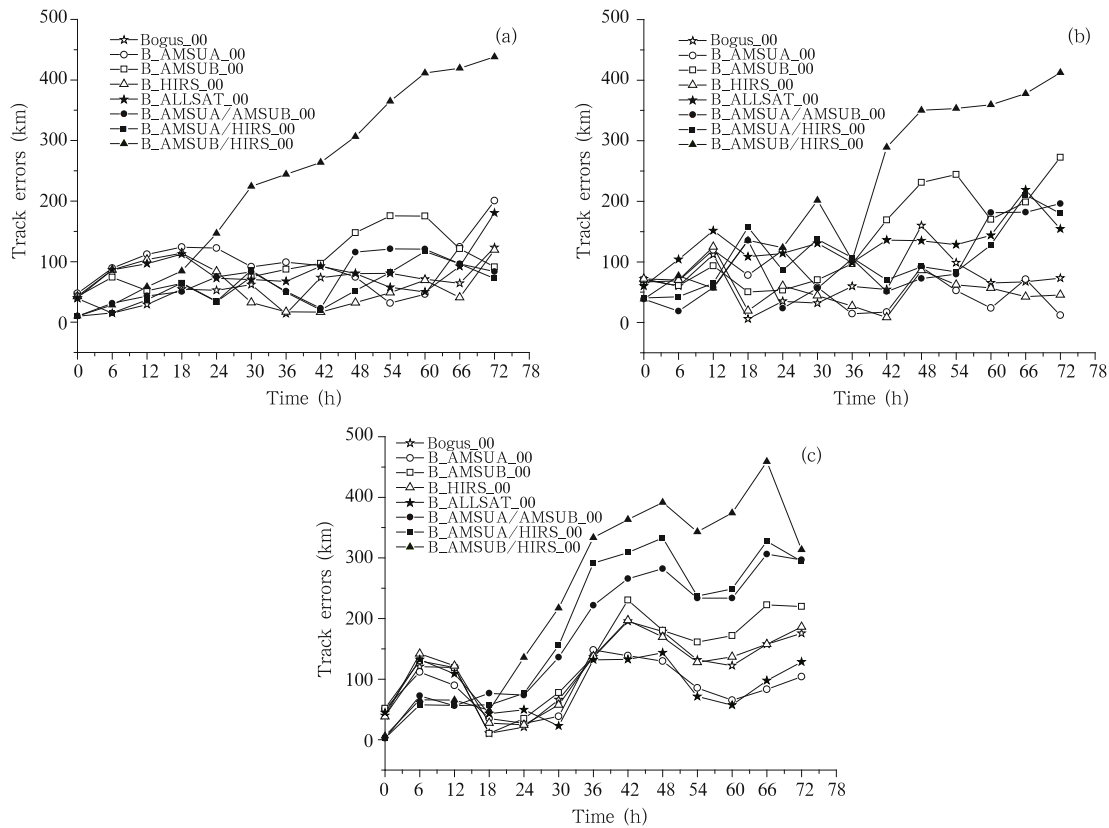


Fig. 11. As in Fig. 4, but for the combined bogus and satellite data assimilation experiments as shown in Table 2.

Figure 11b shows the errors in the typhoon tracks from the assimilation experiments initialized at 0000 UTC 17 July. Assimilating only HIRS data (B_HIRS_06) or only AMSU-A data (B_AMSUA_06) results in smaller errors than any other combination of satellite data. The largest error in these two simulations is less than 130 km. The errors in B_AMSUB_06 are larger than those in Bogus_06 but smaller than those in Ctrl_06 (Fig. 4b), with a maximum error of nearly 270 km. Assimilating all satellite data (B_ALLSAT_06) yields a maximum track error of about 220 km. This track simulation is again more accurate than that offered by Ctrl_06 (Fig. 4b), but less accurate than that by Bogus_06. The simulated track errors in B_AMSUA/AMSUB_06 and B_AMSUA/HIRS_06 are comparable to those in Bogus_06, with maximum errors of less than 200 km in each experiment. The errors in B_AMSUB/HIRS_06 are far larger than those in Bogus_06, with maximum errors of almost 400 km.

Figure 11c shows the errors in the typhoon tracks from the assimilation experiments initialized at 0600 UTC 17 July. Assimilating only one type of satellite data (B_AMSUA_00, B_AMSUB_00, and B_HIRS_00) results in errors consistently less than 220 km. These results are much more accurate than those of Ctrl_12 (Fig. 4c). The errors in B_AMSUA_00 are even smaller than those in Bogus_12. Assimilating all satellite data (B_ALLSAT_12) reduces the simulated track errors still further, with a maximum error of less than 150 km during the 72-h integration. The simulated track errors in B_AMSUA/AMSUB_12, B_AMSUA/HIRS_12, and B_AMSUB/HIRS_12 are all larger than those in the other experiments with bogus data. The maximum errors in these simulations exceed 300 km.

3.3.3 Typhoon intensity simulation

Figure 12 shows the temporal variation of the central SLP of the observed (best track) typhoon and the typhoons simulated by the combined bogus and satellite data assimilation experiments initialized at 0000 UTC 17 July. The introduction of the bogus data significantly affects the simulation of the central

SLP. The initial central SLP of the simulated typhoon is reduced in each experiment relative to the experiments without bogus data, with values much closer to the observed value of 975 hPa. However, this reduction persists too long in all the experiments except B_ALLSAT_06. The central SLP of the simulated typhoons in all the other experiments is much less than the observed toward the end of the 72-h integration period. Unlike the other experiments, B_ALLSAT_06 produces a good simulation of the evolution of typhoon intensity in this case. This indicates that the bogus technique overestimates the intensity of Typhoon Kalmaegi while assimilating all satellite data appears to largely correct this deficiency, so typhoons may be simulated most accurately when the bogus technique is used in tandem with satellite data assimilation.

Figure 13 shows the initial distributions of the 500-hPa wind field and SLP in Bogus_06 along with the changes in these initial distributions after assimilating all satellite data in B_ALLSAT_06. Both experiments are initialized at 0000 UTC 17 July. Figure 13a shows the distribution of the initial wind field at 500 hPa in Bogus_06. Typhoon Kalmaegi is located to the east of the Taiwan Region with a maximum wind speed of about 30 m s^{-1} near the typhoon center. Figure 13b shows the change in the initial wind field at 500 hPa after assimilating all satellite data. Assimilating the satellite data introduces an anticyclonic anomaly centered near 34°N , 113°E , which promotes the initial

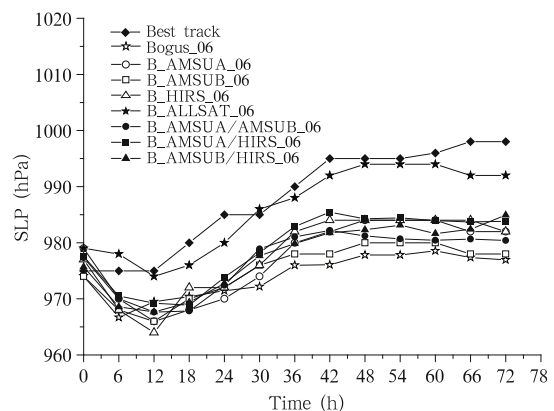


Fig. 12. As in Fig. 5, but for the combined bogus and satellite data assimilation experiments as shown in Table 2.

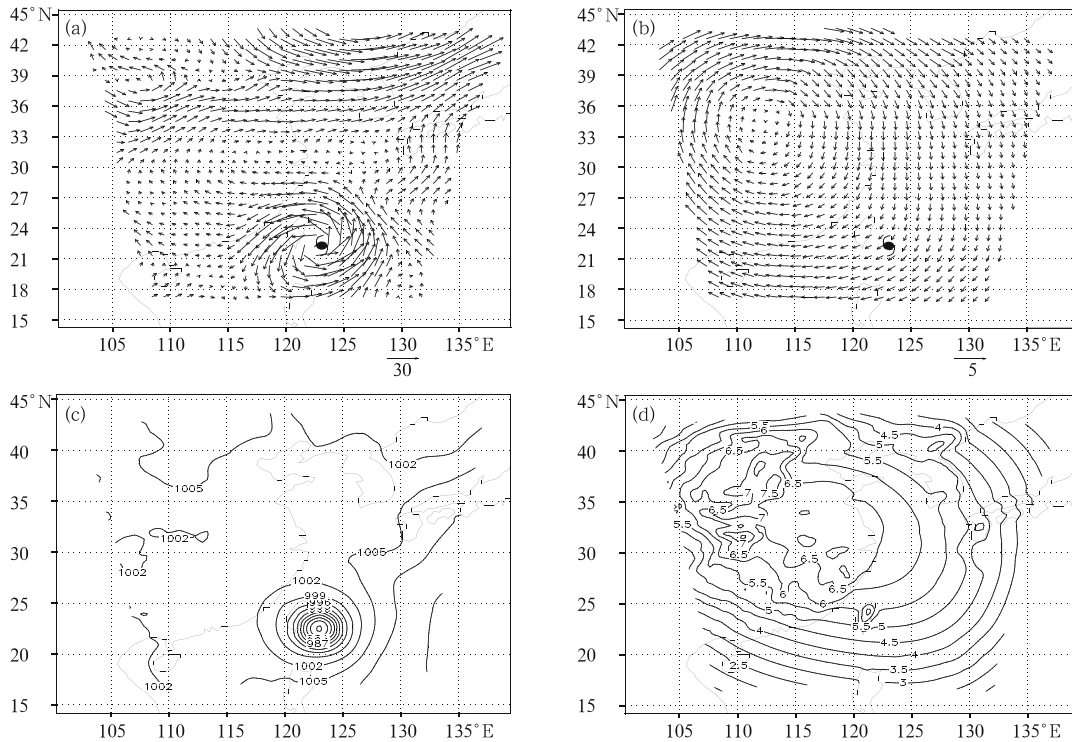


Fig. 13. Distributions of (a) the initial wind field (m s^{-1}) at 500 hPa in experiment Bogus_06, (b) the change in the initial wind field (m s^{-1}) at 500 hPa after assimilating all satellite data (experiment B_ALLSAT_06), (c) the initial SLP field (hPa) in experiment Bogus_06, and (d) the change in the initial SLP field (hPa) after assimilating all satellite data.

westward movement of the typhoon. The change in the wind at the typhoon center is approximately 5 m s^{-1} . Figure 13c shows the distribution of the initial SLP in Bogus_06. The initial typhoon is significantly stronger than that simulated by Ctrl_06. Figure 13d shows the change in the initial SLP fields after assimilating all satellite data. Assimilating the satellite data introduces a weak positive anomaly in SLP (maximum 7 hPa or so) centered near 32°N , 118°E . This change shows that assimilating satellite data weakens the initial typhoon.

Figure 14 shows the initial vertical distributions of temperature and geopotential along 22°N in Bogus_06, along with how these fields are changed by the assimilation of satellite data in B_ALLSAT_06. Figure 14a shows that the initial temperature near the typhoon center typhoon is warmer than the surrounding areas. Figure 14b shows that satellite data assimilation introduces a warm temperature anomaly between 300 and 400 hPa, which may have strengthened

the typhoon. Figure 14c shows that the geopotential near the typhoon center is lower than in the surrounding areas. Figure 14d shows that the geopotential typically increases in the lower and mid troposphere. This change weakens the typhoon while enhances the subtropical high, which helps to promote the initial westward movement of the simulated typhoon as shown in Fig. 8b.

The typhoon track is predominantly determined by three aspects, i.e., the steering by the environmental flow, the interior structure of typhoon, and the interaction between the above two factors. The environmental steering has a greater effect on a relatively weak typhoon. Assimilation of satellite data improves the representation of the steering flow, enabling a better prediction of the typhoon track. The results of these experiments suggest that satellite data assimilation can modify the intensity of the simulated subtropical high and prompt it to extend westward or retreat eastward. These changes in the subtropical high then

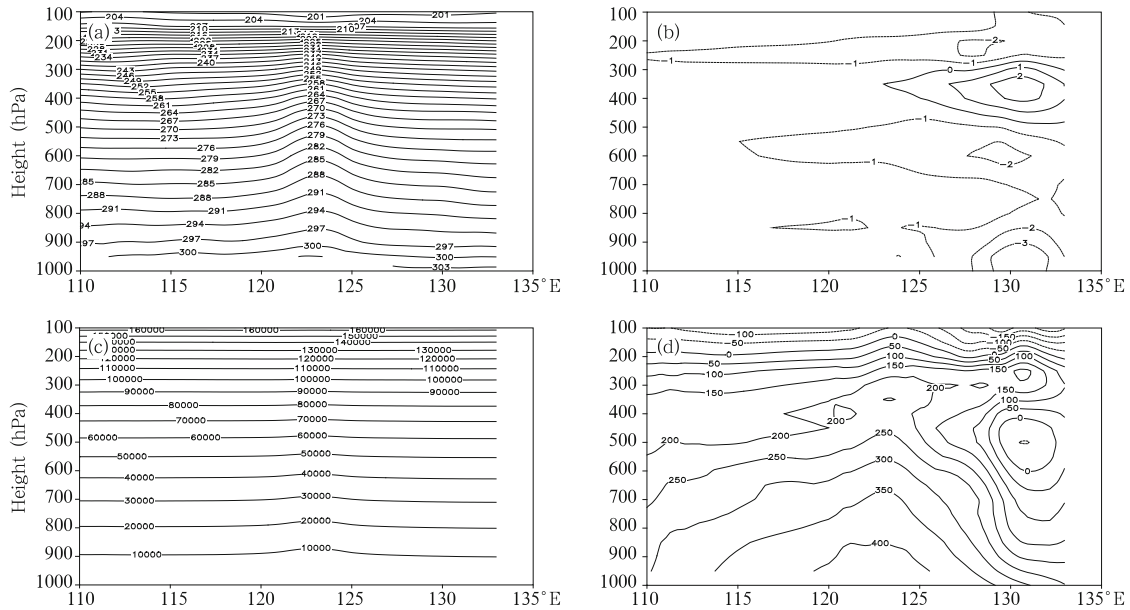


Fig. 14. Vertical distributions along 22°N of (a) the initial temperature field (K) in experiment Bogus_06, (b) the change in the temperature field (K) after all satellite data are assimilated (experiment B_ALLSAT_06), (c) the initial geopotential field ($\text{m}^2 \text{s}^{-2}$) in experiment Bogus_06, and (d) the change in the geopotential field ($\text{m}^2 \text{s}^{-2}$) after all satellite data are assimilated.

influence the movement of the typhoon. However, satellite data assimilation does not have a large impact on the intensity of the simulated typhoon. Combining the bogus technique with satellite data assimilation improves the representation of the interior structure of the typhoon, enabling a better simulation of its intensity. Although the overall results are greatly improved in the bogus data assimilation experiments, this does not mean that bogus data assimilation outperforms satellite data assimilation. The satellite data assimilated in these experiments may contribute more toward improving the environmental conditions than improving the inner structure of the typhoon. The bogus data exerts such a large impact because it changes the inner structure of the typhoon and improves the representation of the initial vortex.

4. Summary and discussion

This study has investigated the effects of assimilating multifold datasets (including bogus data, HIRS data, AMSU-A data, and AMSU-B data) on simulations of Typhoon Kalmaegi (2008). The simulations

are conducted using the Advanced Research WRF model with the 3DVAR technique. Three groups of data assimilation experiments are initialized at three different times, with each experiment assimilating a different combination of datasets. The results are summarized as follows.

(1) The assimilation of satellite data can improve the initial fields and the subsequent simulation of the typhoon, but the relative improvement depends on the exact combination of data assimilated. In this case, assimilating AMSU-A data improves the simulation more than assimilating AMSU-B data or HIRS data. Satellite data assimilation significantly affects the strength and location of the subtropical high, which in turn influences the steering of the typhoon by the environmental flow. Assimilation of AMSU-A data strengthens the subtropical high and shifts it westward, enhancing the initial westward movement of the simulated typhoon and resulting in a simulated track that is closer to the best track.

(2) Direct assimilation of satellite brightness temperature helps to improve the environmental conditions, but does not significantly improve the simulated

intensity of the typhoon. Using the bogus technique together with satellite data assimilation to initialize the typhoon simulation improves not only the environmental conditions but also the structure of the typhoon inner core. These changes yield a more accurate simulation of both the track and intensity of the typhoon.

(3) Assimilation of multifold data improves the representations of the wind and SLP fields both inside and outside of the typhoon, enhances the upper-level warm core within the typhoon, strengthens the subtropical high, and extends the subtropical high toward the west. The assimilation of satellite data contributes primarily toward improving the environmental conditions, and does not significantly improve the structure of the typhoon inner core. The introduction of bogus data primarily affects the structure of the typhoon inner core, resulting in a more accurate representation of the initial vortex.

This study demonstrates that both the bogus technique and satellite data assimilation can independently improve numerical simulations of typhoons. However, in this case, the most accurate simulations result from applying the two techniques in tandem. The results in this paper are informative for ongoing efforts to numerically simulate and predict the evolution of typhoons.

Acknowledgments. The authors gratefully acknowledge Dr. Zhao Juan for constructive Comments and careful examination of the manuscript. The language editor for this manuscript is Dr. Jonathon S. Wright.

REFERENCES

- Chen, H., and W. Y. Pan, 2010: Targeting studies for the extratropical transition of Hurricane Fabian: Signal propagation, the interaction between Fabian and midlatitude flow, and observation strategy. *Mon. Wea. Rev.*, **138**, 3224–3242.
- Cheng Rui, Yu Rucong, Xu Youping, et al., 2011: Impact of cloud microphysical processes on the simulation of Typhoon Rananim near shore. Part II: Typhoon intensity and track. *Acta Meteor. Sinica*, **25**(4), 456–466.
- Chou, M. D., and M. J. Suarez, 1999: A Solar Radiation Parameterization for Atmospheric Studies. NASA Tech. Rep. NASA/TM-1999-10460, 15, 38 pp.
- Eyre, J. R., and H. M. Woolf, 1988: Transmittance of atmospheric gases in the microwave region: a fast model. *Applied Optics*, **27**, 3244–3249.
- Hong, S. Y., Y. Noh, and J. Dudhia, 2006: A new vertical diffusion package with an explicit treatment of entrainment processes. *Mon. Wea. Rev.*, **134**(9), 2318–2341.
- Iwasaki, T., H. Nakano, and H. Sugi, 1987: The performance of a typhoon track prediction model with cumulus parameterization. *J. Meteor. Soc. Japan*, **65**, 555–570.
- Kain, J. S., 2004: The Kain-Fritsch convective parameterization: An update. *J. Appl. Meteor.*, **43**(1), 170–181.
- Kurihara, Y., M. A. Bender, and R. J. Ross, 1993: An initialization scheme of hurricane models by vortex specification. *Mon. Wea. Rev.*, **121**(7), 2030–2045.
- , —, R. E. Tuleya, et al., 1995: Improvements in the GFDL hurricane prediction system. *Mon. Wea. Rev.*, **123**(9), 2791–2801.
- Le Marshall, J. F., L. M. Leslie, R. F. Jr. Abbey, et al., 2002: Tropical cyclone track and intensity prediction: The generation and assimilation of high-density, satellite-derived data. *Meteor. Atmos. Phys.*, **80**(1–4), 43–57.
- Mathur, M. B., 1991: The National Meteorological Center's quasi-Lagrangian model for hurricane prediction. *Mon. Wea. Rev.*, **119**(6), 1419–1447.
- Pu, Z. X., and S. A. Braun, 2001: Evaluation of bogus vortex techniques with four-dimensional variational data assimilation. *Mon. Wea. Rev.*, **129**(8), 2023–2039.
- Wang Guomin, Wang Shiwen, and Li Jianjun, 1996: A bogus typhoon scheme and its application to a movable nested mesh model. *Adv. Atmos. Sci.*, **13**(1), 103–114.
- Wang, Y. F., B. Wang, G. Ma, et al., 2003: Effects of 4DVAR with multifold observed data on the typhoon track forecast. *Chinese Sci. Bull.*, **48**(S2), 93–98.
- , Zhang Haiyang, Wang Bin, et al., 2009: An improved initialization method of typhoon and its 4DVAR experiments. *Sci. Meteor. Sinica*, **29**(1), 1–8. (in Chinese)

- , H. Y. Zhang, B. Wang, et al., 2010: Reconstruct the mesoscale information of typhoon with BDA method combined with AMSU-A data assimilation method. *Adv. Meteor.*, Article ID 346516, 11 pages, doi: 10.1155/2010/346516.
- Xiao, Q. N., X. E. Zou, and B. Wang, 2000: Initialization and simulation of a landfalling hurricane using a variational bogus data assimilation scheme. *Mon. Wea. Rev.*, **128**(1), 2252–2269.
- , L. Q. Chen, and X. Y. Zhang, 2009: Evaluations of BDA scheme using the advanced research WRF (ARW) model. *J. Appl. Meteor. Climatol.*, **48**(3), 680–689.
- Zapotocny, T. H., J. A. Jung, J. F. Le Marshall, et al., 2008: A two-season impact study of four satellite data types and rawinsonde data in the NCEP global data assimilation system. *Wea. Forecasting*, **23**(1), 80–100.
- Zhang, F. Q., Y. H. Weng, J. F. Gamache, et al., 2011: Performance of convection-permitting hurricane initialization and prediction during 2008–2010 with ensemble data assimilation of inner-core airborne Doppler radar observations. *Geophys. Res. Lett.*, **38**, L15810, doi: 10.1029/2011GL048469.
- , and D. D. Tao, 2013: Effects of vertical wind shear on the predictability of tropical cyclones. *J. Atmos. Sci.*, **70**(3), 975–983.
- Zhang, H., J. S. Xue, G. F. Zhu, et al., 2004: Application of direct assimilation of ATOVS microwave radiances to typhoon track prediction. *Adv. Atmos. Sci.*, **21**(2), 283–290.
- Zou, X. L., and Q. N. Xiao, 2000: Studies on the initialization and simulation of a mature hurricane using a variational bogus data assimilation scheme. *J. Atmos. Sci.*, **57**(6), 836–860.
- , —, A. E. Lipton, et al., 2001: A numerical study of the effect of GOES sounder cloud-cleared brightness temperatures on the prediction of Hurricane Felix. *J. Appl. Meteor.*, **40**(1), 34–55.